A multi-scale hybrid long-term morphodynamic model for wave-dominated coasts

Wenyan Zhang [a,*], Ralf Schneider [a], Jan Harff [b]

[a] Institute of Physics, Ernst-Moritz-Arndt-University of Greifswald, Felix-Hausdorff-Str. 6 ,D17489, Greifswald, Germany
[b] Institute of Marine and Coastal Sciences, University of Szczecin, Mickiewicza 18, 70-383 Szczecin, Poland

ARTICLE INFO

ABSTRACT

Process-based modules based on conservative equations to solve the transport of waves, currents and sub-aqueous sediment, and behavior-oriented modules based on empirical descriptions of cliff erosion, bed-load and terrestrial aeolian sand transport are coupled with up-scaling measures and stability-maintaining approaches in a parallel code to simulate decadal-to millennial-scale morphological evolution of wave-dominated coasts. An application to the southern Baltic Sea for a hindcast of Holocene morphogenesis of the Darss–Zingst peninsula demonstrates the robustness of the model. The model is then used to investigate the morphogenesis and evolution of spits in an idealized fetch-limited sandy coastal environment. Evolution of the spit system can be categorized into three periods according to the simulation results. In the early period all initial coastline perturbations are amplified due to the high-angle wave effects. Size competition between adjacent spits starts afterwards. Interaction between adjacent spits dominates the middle period. Smaller spits tend to retrogress due to unbalanced sediment budget and this sediment loss feeds further growth of their larger neighbors. The retrograded spits are either smoothed or evolve into barrier-lagoons, and relatively stable large-scale spits originating from larger spits are developed in the late period. Low-frequency storms impinging from a regular high angle onto the coastline facilitate the development of spits in the early period, but become a hindering factor afterwards. Terrestrial aeolian transport not only plays a key role in stabilizing the spits, but is also revealed as an important factor for long-term coastline erosion.

© 2012 Elsevier B.V. All rights reserved.

1. Introduction

In order to understand physical processes that drive decadal up to millennial scale (referred to as long-term hereafter) coastal morphological evolution numerical models of coastal morphogenesis including different climate scenarios provide a feasible method. Existing coastal morphodynamic models can be classified into three types: 1. process-based; 2. behavior-oriented and 3. hybrid of the former two types. The advantages as well as shortcomings of the first two model types have been widely revealed and discussed (e.g. de Vriend, 2001; Hanson et al., 2003; Fagherazzi and Overeem, 2007). Although high-resolution process-based models are reliable in modeling short-term (from hourly to daily scale) morphodynamics of coastal and shelf areas, direct application of these models to longer-term studies (from annual to millennial scale) is severely restricted and they can hardly perform better than behavior-oriented models. The reason for this originates not only from the numerical errors induced by the solutions for the partial differential equations, but also from insufficient knowledge of the complexity of the natural system. Great efforts have been made by coastal researchers in recent decades to improve the reliability of morphodynamic models. To reduce the errors of process-based models

due to the large amount of iterations needed for a long-term computation, 'reduction' concepts, originally introduced by de Vriend et al. (1993a,b) and Latteux (1995), combined with techniques of morphological update acceleration (Roelvink, 2006) have been implemented in modeling studies (Cayocca, 2001; Wu et al., 2007; Dastgheib et al., 2008). For complex coastal systems hybrid modeling, which combines advantages both of process-based (for physical processes well described by differential equations) and behavior-oriented models (for less-known intrinsic self-organizing systems), has shown its promising perspectives for long-term modeling (Jiménez and Arcilla, 2004; Dissanayake and Roelvink, 2007; Karunarathna et al., 2008).

Among different types of coasts, wave-dominated barrier spits and barrier islands (collectively referred to as barriers hereafter) have the most variable morphology. They are constantly shaped by winds, tides and waves and, on a longer timescale, they can shift landward or seaward due to the oscillations of sea level and variations in the sediment supply (Masetti et al., 2008). Although the general processes for formation and evolution of barriers are described by behavior-oriented conceptual models based on equilibrium concepts and simplified process-based cross-shore models, there are very few morphodynamic models that can be used for 2DH area (based on depth-averaged formulations for hydrodynamics and sediment transport) simulation of long-term morphological evolution of wave-dominated barriers. The construction of a long-term 2DH area morphodynamic model for wave-dominated barriers is a challenging work for coastal researchers as it requires not

* Corresponding author.
E-mail address: wzhang@ipp.mpg.de (W. Zhang).

only resolving all the different processes acting over different scales for morphological evolution but also maintaining the computational stability especially on the water–land interaction area, which is the most variable part of a wave-dominated barrier. This includes the shallow sub-aqueous area which is permanently under the influence of wave action and the low-altitude terrestrial area which is affected by aeolian transport during calm weather periods and strong waves during storm surges. For the former problem, a multi-scale concept has to be integrated into the model for coupling the different modules which calculate the processes at their corresponding temporal and spatial scales. Approaches for maintaining the computational stability of a process-based model in a long-term simulation need to be investigated and integrated into the model to solve the latter problem.

Recently Zhang et al. (2010, 2011a,b) presented a modeling methodology for long-term morphological evolution of wave-dominated coasts based on a multi-scale morphodynamic model. The model consists of 8 modules which calculate the processes of interest at different scales. The 2DH current module, the wave module, the bottom boundary module, the sub-aqueous sediment transport module and the cliff erosion module are real-time calculation modules which solve the short-term processes. A bathymetry update module and a long-term control module, in which the 'reduction' concepts and techniques of morphological update acceleration are implemented, are integrated to extend the effects of short-term processes over longer time periods. Promising results were obtained in the model application to a hindcast of 300 years' morphological evolution of the Darss–Zingst peninsula in the southern Baltic Sea. Long-term residual effects of waves as well as short-term effects of storms are revealed as the dominant factors driving the morphological evolution of the research area during the last several centuries (Zhang et al., 2010). Although good agreement between simulation results and measured data is shown for the major part of the coast, some key areas such as the spit and the newly-formed barrier are not satisfactorily reproduced. Analysis of the results indicates that inclusion of terrestrial aeolian sand transport, which is responsible for dune formation and migration, is necessary in a long-term model for wave-dominated barriers for describing better the water-land transition process. The aim of this paper is to introduce further improvements of the existing long-term morphodynamic model by including terrestrial aeolian sand transport effects. This model is then used for a study of the natural morphogenesis of wave-dominated sandy coasts. In Section 2 a brief description of the original model and further model improvements is introduced. Approaches for guaranteeing the computational stability of the model are also described. An application of the model to a real coast is presented in Section 3, and a study of an idealized coast is given in Section 4. Simulation results are critically discussed in Section 5, before the conclusions are drawn in Section 6.

2. The model

2.1. Brief description of the original model

The original multi-scale morphodynamic model for long-term evolution of wave-dominated coasts consists of 8 main modules to describe different physical processes that drive the morphological evolution of the coastal environment. The modules are:

(1) a 2DH (two-dimensional vertically integrated) circulation module based on shallow-water equations,
(2) a wind-induced wave module based on momentum conservation equations,
(3) a bottom boundary layer (BBL) module based on the Grant–Madsen formulation (Grant and Madsen, 1979),
(4) a sub-aqueous sediment transport module based on a process-based formulation of suspended transport of cohesive and non-cohesive sediment and a behavior-oriented formulation of bed-load sediment transport,

(5) a cliff erosion module based on a behavior-oriented formulation (Zhang et al., 2010),
(6) a nearshore storm module based on the XBeach model (Roelvink et al., 2009),
(7) a bathymetry update module based on the technique of morphological update acceleration (Roelvink, 2006) and approaches for maintaining the computational stability, and
(8) a control function set for up-scaling of the short-term effects.

For details of the modules the reader is referred to Zhang et al. (2010, 2011b).

2.2. The terrestrial aeolian sand transport module

The terrestrial aeolian sand transport module follows an empirically modified Bagnold-type formulation (Lettau and Lettau, 1978). Aeolian transport is only activated when the bed shear velocity exceeds a critical shear velocity. The total volumetric transport rate $Q\,(\mathrm{m^2\,s^{-1}})$ accounting for the bed-slope effect is given by:

$$Q = f_2(d)\frac{\rho}{\rho_s g}\left(1 - \frac{u_{*cr}}{u_{*wind}}\right)^{0.25} u_{*wind}^3 (1 - \tan\beta/\tan\varphi), \tag{1}$$

where ρ is the air density ($=1.25\ \mathrm{kg\ m^{-3}}$), $\rho_s = 2650\ \mathrm{kg\ m^{-3}}$ is the sand density, g is gravitational acceleration, u_{*cr} is the critical shear velocity for initiation of motion of sands, u_{*wind} is the bed shear velocity of winds, $\tan\beta$ represents the local bed slope, $\tan\varphi = 0.62$ ($\varphi = 32°$) is the internal friction angle of the grains in the bed, $f_2(d)$ is a function of mean grain size (d_{50}) expressed by:

$$f_2(d) = 1.49 + 5e^{-0.5\left(\ln\left(d/1.53D_{ref}\right)/0.56\right)^2}, \tag{2}$$

where $D_{ref} = 0.25$ mm is defined as the reference grain size.

The critical shear velocity for the initiation of sand motion u_{*cr} is calculated by

$$u_{*cr} = A[gd(\rho_s - \rho)/\rho]^{0.5}, \tag{3}$$

where A is a proportionality coefficient. A is a constant (0.1 at the fluid threshold, 0.085 during saltation) according to Bagnold's suggestion. $A = 0.09$ is adopted in the model according to the study of Dong et al. (2003). A uniform mean grain size of sand $d_{50} = 0.33$ mm is used for the experiments in Section 4.

The wind shear velocity at the land–air interface u_{*wind} is given by:

$$u_{*wind} = \frac{\kappa U_z}{\ln(z/z_0)}, \tag{4}$$

where U_z is the wind speed at z meter above the local cell. A uniform hourly-updated wind speed U 10 m above mean sea level for the whole domain is used in our simulation. z for a local terrestrial cell is determined by the difference between the height of the cell and 10 m above mean sea level. $z = 0.5$ is specified for the cells higher than 9.5 m above mean sea level. $\kappa = 0.41$ is von Karman's constant, z_0 is the aerodynamic roughness height which is typically between 10^{-4} and 10^{-2} m. We used in our simulation $z_0 = 0.125$ mm.

In the model the total volumetric transport rate Q is represented by two components (Q_x and Q_y) along the x coordinate and y coordinate, respectively. With the value of Q_x and Q_y the bed elevation update is given by:

$$(1-p)\frac{\partial z_b}{\partial t} + \frac{\partial Q_x}{\partial x} + \frac{\partial Q_y}{\partial y} = 0, \tag{5}$$

where p is the porosity of sands and z_b is the bed elevation relative to mean sea level.

As the volumetric transport rates are determined by the wind shear velocity, the differential terms for these two values on the left hand side of Eq. (5) are solved with finite differences using a first order upwind scheme with the bed elevations at the old time step and the corresponding wind shear velocities at the new time step. Because morphological update acceleration is applied (Zhang et al., 2010), a variable morphological factor f is used in the morphology update. Eq. (5) is thus further expressed as:

$$z_b^{n+1} = z_b^n + \frac{f}{1-p} \int_n^{n+1} \left(\frac{\partial Q_x}{\partial x} + \frac{\partial Q_y}{\partial y} \right). \tag{6}$$

Based on the fact that the evolution of bed elevation is slower than aerodynamics and hydrodynamics, a much larger time step (compared to the hydrodynamic time step in the model) is used for the bed elevation change in the bed-load model. The time step used in the calculation of bed level change is not fixed but varies with time, depending on the value of f (which is explicitly related to the strength of the wind field). As our model is not designed to solve the complete aerodynamics described by Navier–Stokes equations, the time step for the bed elevation update is not limited by the Courant criterion but by a predefined value ε which is considered as a critical value that significantly influences the local aerodynamics. $\varepsilon = 0.5$ m is used in our simulation. The integration in Eq. (6) is performed with a fourth-order Runge–Kutta method, in which the time step is adjusted automatically to satisfy the predefined criterion.

Exchange of sediment at the interface between the water and the land area is not only determined by aeolian effects but also by the wetting of sediment caused by wave swash, which is not resolved in our model. We parameterize this in a simple way by reducing the transport rate at the terrestrial boundary cells adjacent to water area. Sensitivity studies (see supplementary online material) indicate that a reduction to 1/5 of the calculated value obtained from Eq. (1) at these boundary cells is able to maintain a smooth evolution of the coastline. The effect of vegetation on the aeolian transport is taken into account by using a simple linear formulation as follows:

$$u_{*,wind,i,j} = (1-B)u_{*,wind,i,j}. \tag{7}$$

The value of u_{*wind} on the right hand side of the equation is obtained from Eq. (4). B is the fraction of vegetated area in the cell. The value of B for a local terrestrial cell is a function of the cell age and the volume of sand it has received from the last period. The initial age of all terrestrial cells is set to 0 at the beginning of simulation in the experiments. A two-dimensional array named '$Dry\_cell\_age(i,j)$' is defined in the model to record the age of every terrestrial cell for the calculation of vegetation effects. The time counter will be increased for a cell as long as it remains above mean sea level. The value will be set to zero if the cell switches to a water cell with an elevation below mean sea level. Based on these criteria, B is given by:

$$B_{i,j} = 0, Dry\_cell\_age(i,j) < k \text{ years}$$
$$B_{i,j} = \sum_{i=1}^{N} \left[0.5 \times \left(1 - \frac{S_{N-1,i,j}}{\Delta x_{i,j} \Delta y_{i,j}} \right) \right]^i, \quad N = \text{int}(Dry\_cell\_age(i,j)/k). \tag{8}$$

Here $S_{N-1,i,j} = V_{N-1,i,j}/0.5$ m represents the sand area that the cell received from the last period (k years), where $V_{N-1,i,j}$ is the received sand volume. 0.5 m is set as the average height of the vegetation cover, which is assumed to be mainly composed of grass and dwarf shrubs. The symbol 'int' in Eq. (8) indicates the integer part of the real number in the bracket; k is a user-defined parameter. $k = 50$ is used in our simulation.

Wherever the local slope (β) exceeds the internal friction angle ($\varphi = 32°$) of the sand grains, the surface becomes unstable and avalanches occur in the direction where the slope exceeds the critical

value in the model. Avalanches are regarded as instantaneous since their timescale is much smaller than that of bed elevation change caused by dune migration, thus the effect of avalanches is integrated into the bed elevation update at every time step whenever it happens. For example, the local bed slope in x-direction is given by:

$$\frac{\partial z_b}{\partial x} = \frac{z_{b,i+1,j} - z_{b,i,j}}{\Delta x}. \tag{9}$$

The bed elevation change (Eq. 6) with a following avalanche effect is then calculated according to the XBeach model (Roelvink et al., 2009):

$$\Delta z_b^{n+1} = \min \left(\left(\frac{\partial z_b^{n+1}}{\partial x} - 0.62 \right) \Delta x, 0.5 \text{ m} \right), \frac{\partial z_b^{n+1}}{\partial x} > 0.62$$
$$\Delta z_b^{n+1} = \max \left(\left(\frac{\partial z_b^{n+1}}{\partial x} + 0.62 \right) \Delta x, -0.5 \text{ m} \right), \frac{\partial z_b^{n+1}}{\partial x} < -0.62. \tag{10}$$

A maximum bathymetrical change after one avalanche event (0.5 m) is introduced in Eq. (10) to prevent the generation of large shockwaves in the computation. The setting of 0.5 m corresponds to the critical value ε described previously. The bed elevation at the $n+1$ time step is then updated as:

$$z_{b,i,j}^{n+1} = z_{b,i,j}^{n+1} + \Delta z_b^{n+1}$$
$$z_{b,i+1,j}^{n+1} = z_{b,i+1,j}^{n+1} - \Delta z_b^{n+1}. \tag{11}$$

The first term on the right hand side of Eq. (11) is obtained from Eq. (6). To account for continuity, e.g. when sands from terrestrial cells are deposited in the water area, the bed elevation of the water cell is also updated.

As all modules are coupled in a parallel structure (a detailed description of the parallel coupling is given in Section 2.3), this allows us to separate computations of the modules on different grids. In the long-term model, computations of the modules related to hydrodynamics and sub-aqueous sediment transport (except the nearshore storm module which uses a local grid at the coastline with higher resolution) are carried out on a uniform grid system (Fig. 4b). The long-term model uses the staggered 'C-grid' discretization scheme, and sediment transport rates are calculated at the centre of the grid cells (e.g. point C in Fig. 1). Calculations of hydrodynamics and sub-aqueous sediment transport on the water cells do not interfere with calculations of aeolian transport on the terrestrial cells, the only interaction is in the bed-elevation update module. Thus, a fast grid-subdivision scheme is integrated into the aeolian transport module to increase the spatial resolution for a better description of the dune evolution. The fast sub-division scheme is based on a simple quartering division of the terrestrial cells (as illustrated in Fig. 1). Coordinates of the central points in the new terrestrial grid (dashed lines in Fig. 1) after the subdivision can be easily obtained from the coordinates of the corner points (e.g. X11, X12, X21, X22) and
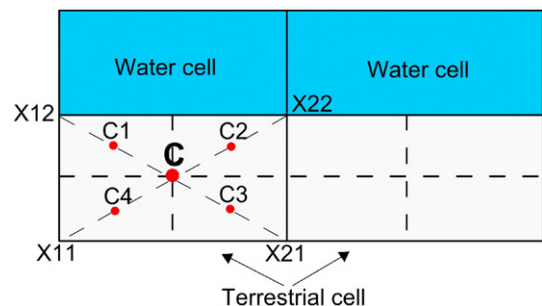

Fig. 1. Sketch of the grid-subdivision scheme.

the central point (e.g. C) in the original grid. A factor of four of increase of the spatial resolution is obtained by each subdivision. Higher resolution can also be achieved with further subdivisions. For a balance of CPU time with other modules, only one step subdivision (i.e. a factor of 4 of increase of spatial resolution) is used in our simulation.

2.3. A parallel coupling structure

One factor hindering the development of a process-based long-term model is the limit in calculation efficiency. Without a parallel computational structure process-based long-term modeling of coastal morphology is extremely time-consuming even on modern high-performance computers, and thus not realistic to serve as a tool for research. In an application on the Darss–Zingst Peninsula (Zhang et al., 2010) with a computational grid of 242×162 and a maximum spatial resolution of 100 m×100 m, the total time needed in a serial coupling model for a simulation of 300 years is about 106 h (on a computer platform with Intel(R) Xeon(R) CPU E5530@2.40 GHz and a memory of 32 GB). The calculation efficiency will be hardly acceptable if such a serial coupling model is applied to a millennial-scale simulation, in which a large number of sensitivity runs are needed.

A parallel coupling structure (Fig. 2) is implemented into the long-term model to improve the calculation efficiency. In the parallel code, computation of each module is assigned to an independent core. These cores run parallel and do not interfere with one another. A master core coordinates the whole group of cores (illustrated by the dashed box in Fig. 2). It is responsible for the following tasks: (1) reading external input files; (2) initializing all parameters; (3) distributing initial conditions to each core; (4) synchronizing all cores at every time step; (5) collecting results from each core after every time step of computation; (6) distributing the latest results to each core to start the next time step of computation; and (7) updating the bathymetry and outputting the results to external files. With this parallel coupling, the total time needed for a long-term simulation is determined by the core which consumes most CPU time (in our case the wave module). This is more efficient than a serial coupling structure in which the simulation time is determined by the sum of the CPU time consumed by every module. A factor of five improvement in calculation efficiency is obtained in the parallel model.

In the parallel coupling structure, each module uses the results of the last time step from other modules as input to calculate its own values for the current time step. For example, the 2DH current module uses the wave parameters (e.g. the significant wave height $HSIG_{t-1}$) obtained from the last time step of the calculation (named time step $t-1$) in the wave module as external conditions to calculate the flow velocities at time step t. This is different from the serial coupling structure in which the 2DH module uses the mean value of two sequential time steps (e.g. $(HSIG_{t-1} + HSIG_t)/2$ for significant wave height) as external conditions to calculate the flow velocities at time step t. Although the computation strategy differs, the relative error is within 3% in the application on the Darss–Zingst Peninsula for a simulation of 300 years for the two coupling structures. This is due to two facts: (1) The second order accurate finite difference scheme in the model is consistent, convergent and stable under the Courant–Friedrichs–Levy condition; and (2) The gradient of bathymetrical change between two adjacent time steps is limited to a low level by the stability-maintaining approaches (which will be described in the next section) in the computation to avoid shock-waves being induced by strong hydrodynamics.

2.4. Approaches for maintaining computational stability

Computational stability is a key issue in the construction of a long-term model as the truncation errors can pile-up during a large number of iterations and finally lead to large bias in the results. Several methods were implemented in the practical application on the Darss–Zingst peninsula to guarantee a stable coastline evolution (Zhang et al., 2010). Besides those measures introduced for the southern Baltic coast, three additional approaches are implemented into the model to avoid spurious oscillations in the morphological evolution of a generalized wave-dominated coastal environments.
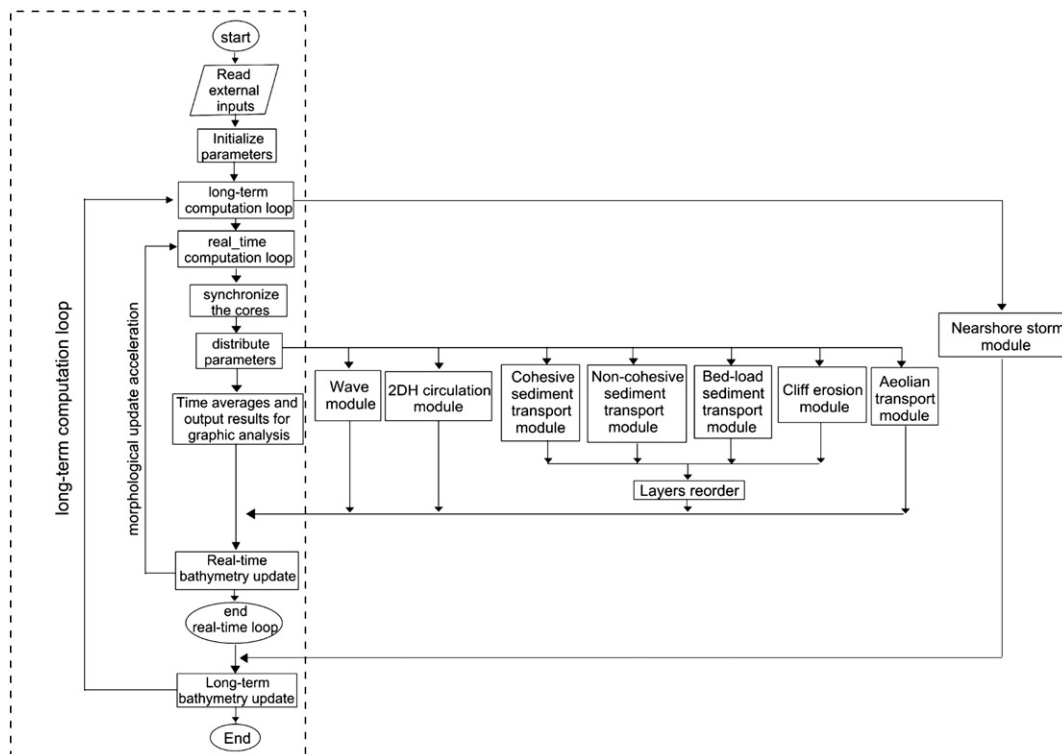

Fig. 2. A general flowchart of the parallel coupling model structure. Dashed box indicates tasks of the master core.

2.4.1. Variable morphological update acceleration

Morphological update in our long-term model for the Darss–Zingst peninsula is mainly based on two approaches: the 'online approach' and 'straightforward extrapolation' (Zhang et al., 2010). Morphological update acceleration factors are introduced in both approaches to up-scale the morphological evolution. These two approaches can also be implemented for other wave-dominated coasts considering the specific morphodynamic conditions of the research area. Here, we use the wind-wave conditions illustrated in Fig. 4c as an example to describe the use of variable morphological update acceleration in a long-term model.

The morphological update acceleration factor f is used to reduce the computational time. In the model the flow, sediment transport and bathymetrical update are all run with the same small time steps and the calculated bed change after each time step is multiplied by f, so that after a simulation of 1 day the model has, in fact, produced the morphological change for f days. However, spurious oscillations might be induced if the value of f is too large, especially for a high-energy hydrodynamic environment. This brings a need for different parameterizations of f for different hydrodynamic conditions. $f = 1$ is used in our model for storm simulations, which means no morphological update acceleration is implemented. For normal wind conditions, a variable f is used in order to reduce the bed level change caused by a combined effect of the westerly winds and easterly winds without violating the basic physics and statistics of wind conditions. A more detailed procedure is that first the model is used to calculate the morphological change induced by a series of westerly winds (usually covering a time span of several days, referred to as a 'westerly wind event' hereafter) with a fixed value of f_1, then the morphological change induced by a series of easterly winds is calculated with another value of f_2. The criterion for the choice of f_2 is that the maximum net sediment transport flux induced by these two wind events is limited to a small value (e.g. at the order of magnitude of $10 \text{ m}^3/\text{m/a}$). In this case, f_1 series of westerly winds and f_2 series of easterly winds are simulated and the resultant morphological change is kept to a low level. This procedure is continued until all representative wind series are simulated. The values of f_1 and f_2 should not violate the statistics of wind distribution in the research area.

2.4.2. Additional diffusion term for the sediment transport

Introduction of a diffusion-like term in the Exner equation to damp numerical oscillations in a morphodynamic model has been proposed by several researchers (Cayocca, 2001; Johnson and Zyserman, 2002; Fortunato and Oliveira, 2007). Following the study by Watanabe et al. (1986), it is apparent that the sediment grains tend to move downward when the local bed slope (sub-aerial as well as sub-aqueous) becomes steep enough. Thus, the effect of bottom slope should be taken into account in the bed elevation change. Effects of local bottom slope on the sediment transport rate are already included in the aeolian sand transport module and the sub-aqueous bed-load sediment transport module. An additional isotropic diffusion term which reflects gravity effects caused by the local bed slope is introduced in the sub-aqueous suspended sediment transport modules, and the influence of the diffusion term in the bed-elevation update is reflected by a modified form of Eq. (5):

$$(1-p)\frac{\partial z_b}{\partial t} + \frac{\partial Q_x^*}{\partial x} + \frac{\partial Q_y^*}{\partial y} = 0, \tag{12}$$

where Q_x^* and Q_y^* represent the sediment transport flux including the additional diffusion effects in x and y direction, respectively, and are given by:

$$Q_{sx}^* = Q_{sx} + \varepsilon_{sxx}|Q_{sx}|\frac{\partial z_b}{\partial x} + \varepsilon_{sxy}|Q_{sx}|\frac{\partial z_b}{\partial y}$$
$$Q_{sy}^* = Q_{sy} + \varepsilon_{syy}|Q_{sy}|\frac{\partial z_b}{\partial y} + \varepsilon_{syx}|Q_{sy}|\frac{\partial z_b}{\partial x}. \tag{13}$$

Values of the dimensionless diffusion coefficients ε_{sx*}, ε_{sy*} are given by Antunes do Carmo and Seabra-Santos (2002):

$$\varepsilon_{sxx} = \varepsilon_{sxy} = \varepsilon_s \left|\frac{u}{w_f}\right|$$
$$\varepsilon_{syy} = \varepsilon_{syx} = \varepsilon_s \left|\frac{v}{w_f}\right| \tag{14}$$

where u and v indicate flow velocities in x and y direction, respectively, and w_f is the settling velocity of sediment particles. $\varepsilon_s \approx 0.01$–$0.03$ is proposed in the literature. The upper limit of the value $\varepsilon_s = 0.03$ is used in our simulation.

2.4.3. Euler–WENO approach

The Euler–WENO (Weighted Essentially Non-Oscillatory) approach is based on a first order forward time-stepping together with a WENO scheme for spatial discretization. The WENO scheme (Liu et al., 1994) originated from an ENO (Essentially Non-Oscillatory) scheme developed by Harten et al. (1987) whose key idea was to use the smoothed stencil among several candidates to approximate the sediment fluxes at cell interfaces $(i \pm 1/2, j)$ and $(i, j \pm 1/2)$ to a high order of accuracy and to avoid at the same time spurious oscillations near shocks or discontinuities. WENO extends this by taking a weighted average of the candidate stencils to obtain local smoothness.

Adoption of the Euler–WENO approach to our model is based on the studies by Long et al. (2008) and Chiang et al. (2010) in which the stability and performance of several finite difference schemes for removal of spurious oscillations in long-term sediment transport simulation were investigated. Long et al. (2008) studied the evolution of periodic alternating sand bars in a rectangular open channel under the gravity wave and flow condition. Chiang et al. (2010) applied the tests on a sandy beach with a complex topography. Advantages of the Euler–WENO approach were proven in both studies in comparison to other classical schemes such as the Lax–Wendroff, FTCS (Forward Time, Central Space) and upwind schemes. A successful use of the Euler–WENO approach in wave phase-resolving sediment transport models for a wave-dominated coastal environment was also demonstrated. Technical details about the Euler–WENO approach are given in Long et al. (2008) and Chiang et al. (2010); here we introduce only the basic ideas of the approach.

A key element of the Euler–WENO approach is to split the sediment transport rates Q_x and Q_y into two parts which are associated with bed form propagation in the positive and negative directions, respectively:

$$Q_x = Q_x^+ + Q_x^-$$
$$Q_y = Q_y^+ + Q_y^-. \tag{15}$$

The two terms $\frac{\partial Q_x}{\partial x}$ and $\frac{\partial Q_y}{\partial y}$ in Eq. (5) are thus approximated by:

$$\frac{\partial Q_x}{\partial x} = \frac{\hat{Q}_{x,i+1/2,j} - \hat{Q}_{x,i-1/2,j}}{\Delta x_i}$$
$$\frac{\partial Q_y}{\partial y} = \frac{\hat{Q}_{y,i,j+1/2} - \hat{Q}_{y,i,j-1/2}}{\Delta y_i}. \tag{16}$$

The next step is to estimate $\hat{Q}_{x,i+1/2,j}$, $\hat{Q}_{x,i-1/2,j}$, $\hat{Q}_{y,i,j+1/2}$ and $\hat{Q}_{y,i,j-1/2}$, which are approximations of the transport rates at cell interfaces $(i \pm 1/2, j)$ and $(i, j \pm 1/2)$. According to Eq. (15), these four quantities are split again into left-biased and right-biased flux, respectively. Here we take $\hat{Q}_{x,i+1/2,j}$ for example to briefly explain the WENO procedures, $\hat{Q}_{y,i,j+1/2}$ is calculated in the same manner. The biased flux terms for location $i - 1/2$ ($\hat{Q}_{x,i-1/2,j}$) and $j - 1/2$ ($\hat{Q}_{y,i,j-1/2}$) are calculated following the procedure by simply shifting i and j backward for one spatial step, respectively.

$\hat{Q}_{x,i+1/2,j}$ is given by:

$$\hat{Q}_{x,i+1/2,j} = \hat{Q}^-_{x,i+1/2,j} + \hat{Q}^+_{x,i+1/2,j}.$$

The left-biased flux is calculated by:

$$\hat{Q}^-_{x,i+1/2,j} = \omega_{x1}Q^1_{x,i+1/2,j} + \omega_{x2}Q^2_{x,i+1/2,j} + \omega_{x3}Q^3_{x,i+1/2,j}, \quad C_{x,i+1/2,j} \geq 0$$

$$\hat{Q}^-_{x,i+1/2,j} = 0, \quad C_{x,i+1/2,j} < 0 \qquad (17)$$

and the right-biased flux is calculated by:

$$\hat{Q}^+_{x,i+1/2,j} = \tilde{\omega}_{x1}\tilde{Q}^1_{x,i+1/2,j} + \tilde{\omega}_{x2}\tilde{Q}^2_{x,i+1/2,j} + \tilde{\omega}_{x3}\tilde{Q}^3_{x,i+1/2,j}, \quad C_{x,i+1/2,j} < 0$$

$$\hat{Q}^+_{x,i+1/2,j} = 0, \quad C_{x,i+1/2,j} \geq 0 \qquad (18)$$

where $Q^1_{x,i+1/2,j}$, $Q^2_{x,i+1/2,j}$, $Q^3_{x,i+1/2,j}$, $\tilde{Q}^1_{x,i+1/2,j}$, $\tilde{Q}^2_{x,i+1/2,j}$ and $\tilde{Q}^3_{x,i+1/2,j}$ are candidate stencils obtained by expansion of the Taylor series for estimating Q_x at location $(i+1/2,j)$ with third order accuracy; $C_{x,i+1/2,j}$ is the bed form propagation phase speed at location $(i+1/2,j)$ in x direction. We only need to obtain the sign of the bed form propagation phase speed in Eqs. (17) and (18) by calculating the Roe speed to proceed. This defines the advantage of Euler–WENO in comparison with central difference schemes and upwind schemes, in which the exact values of the bed form propagation phase speeds are required, which are not easy to estimate in many instances (Long et al., 2008).

The weight parameters $\omega_{xk}(k=1,2,3)$ in Eq. (17) and $\tilde{\omega}_{xk}(k=1,2,3)$ in Eq. (18) are carefully chosen to meet the following criteria: (1) $\hat{Q}_{x,i+1/2,j}$ obtained from Eqs. (17) and (18) is fifth order accurate approximation of $Q_{x,i+1/2,j}$ at location $(i+1/2,j)$; and (2) no spurious oscillations occur while $\hat{Q}_{x,i+1/2,j}$ is discontinuous near $(i+1/2,j)$.

With the results of $\hat{Q}_{x,i+1/2,j}$, $\hat{Q}_{x,i-1/2,j}$, $\hat{Q}_{y,i,j+1/2}$ and $\hat{Q}_{y,i,j-1/2}$ for each inner grid cell, the bed elevation change at (i, j) is calculated by a first order forward time-stepping:

$$(1-p)\frac{z^{n+1}_{b,i,j}-z^{n+1}_{b,i,j}}{\Delta t} + \frac{\hat{Q}_{x,i+1/2,j}-\hat{Q}_{x,i-1/2,j}}{\Delta x} + \frac{\hat{Q}_{x,i,j+1/2}-\hat{Q}_{x,i,j-1/2}}{\Delta y} = 0. \quad (19)$$

The Euler–WENO approach gives first order accuracy $O(\Delta t)$ in time and fifth order accuracy $O(\Delta x^5, \Delta y^5)$ in space.

3. Model application to a real coast

The model was applied to study the Holocene morphogenesis of the Darss–Zingst peninsula in the southern Baltic Sea. A digital elevation model (DEM) describing the paleo-morphology of the research area at 6000 cal. yr BP after the maxima Littorina transgression (Fig. 3) was reconstructed on the basis of interpretation of dated sediment cores, seismo-acoustic profiles, an isostatic map and an eustatic scenario for Holocene mean sea-level change of the southern Baltic Sea (Harff et al., 2011). With the paleo-DEM, the eustatic curve, the isostatic map, a sediment map of the research area and validated modules (Zhang et al.,
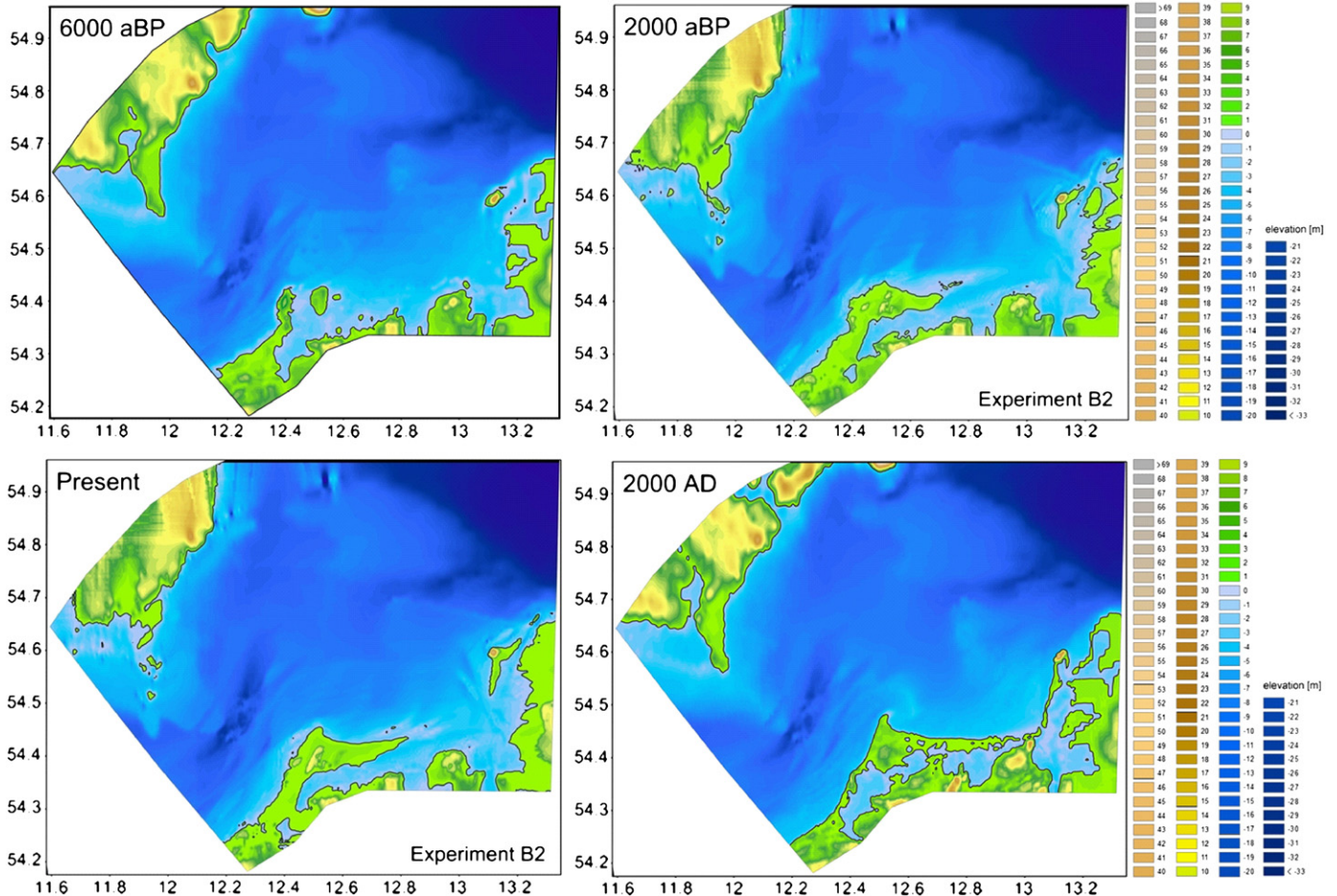

Fig. 3. Reconstructed Holocene morphogenesis of the Darss-Zingst peninsula. Upper left: reconstructed paleo-DEM at 6000 aBP as the initial DEM for simulation; Upper right and bottom left: simulation results; Bottom right: measured modern DEM.

2011b), the model was applied to hindcast the morphological evolution of the Darss–Zingst peninsula from 6000 cal. yr BP to present without taking into account anthropogenic influence. Representative wind series (see supplementary online material), which were initially obtained from statistical analysis of hindcast data by paleo-climate modeling (Hünicke et al., 2010) and subsequently calibrated by sedimentological proxy data from the Baltic Sea and sensitivity studies, serve as driving input conditions of the model. Sedimentological studies of the research area by Lampe (2002) and Schumacher (2002) serve as a reference for model calibration. Qualitative agreement is shown between the simulation results and the reality (Fig. 3). Although errors exist in details of the coastline configuration, the main morphological features of the barrier (such as the spits) are reasonably replicated and several driving mechanisms are discovered from the simulation results to explain the morphological evolution of the coastal system in different periods (Zhang et al., submitted for publication). For a detailed description of the numerical study on the Holocene morphogenesis of the Darss–Zingst peninsula the reader is referred to Harff et al. (2011) and Zhang et al. (submitted for publication).

4. Model application to an idealized coast

4.1. Model set-up

The validated model is used to investigate the morphogenesis and evolution of spits, which are common features in wave-dominated coasts. An idealized coastal environment (Fig. 4b) is designed as a starting point for the simulation. A series of small-scale perturbations (red circles in Fig. 4b) are introduced at the initial coastline to serve as triggers of spit formation. Wind is the only driving force for the whole system. A synthetic wind spectrum serving as model input is designed to induce a dominant nearshore wave spectrum that approaches the coastline in oblique incident angles greater than 45° (named high-angle hereafter). Wind vectors are generated following the procedures introduced in Zhang et al. (2011a) with a Weibull parameter setting ($k = 2.2$, $\lambda = 7.5$) and a directional distribution shown in Fig. 4c. The Weibull

parameter setting of the synthetic wind series corresponds to a moderate wind climate, which allows the use of a relatively large morphological up-date acceleration factor ($f = 120$) in the computation, in order to save the CPU time. 720 hourly wind elements (i.e. covering a whole month) are generated and the wind sub-groups are arranged in an order that a westerly sub-group is followed by an easterly sub-group. No division of the wind sub-groups is implemented. The monthly wind series simply repeats as input in every loop of the long-term computation.

Two coupled grids are used. A rectilinear, equidistant regional grid (Fig. 4a) covering a coastal area of 160 km×40 km with a spatial resolution of 500 m×500 m is used to provide open boundary conditions for a local grid. Only waves and currents are simulated on the regional grid. A rectilinear, non-equidistant local grid with a maximum resolution of 100 m×100 m at the coastline area is designed to simulate the long-term coastal morphological evolution. Resolution of the local grid decreases linearly toward offshore to a resolution of 100 m×1000 m. The initial morphology is homogenous alongshore except at the coastline perturbations. The slope of the cross-shore bathymetry is 0.01 from 0 m to 5 m (contour line), 0.0035 from 5 m to 12 m and 0.003 from 12 m to 25 m. The terrain part of the model domain has a slope of 0.005 from the waterline to 1 m above mean sea level (named MSL hereafter), and is then randomly distributed with the height between 1 m and 2 m above MSL. The MSL remains fixed during simulation. The whole model domain is covered by an erodible sediment layer of 10 m thickness. The sediment is composed of 15% coarse sand ($d_{50} = 0.5$ mm), 70% fine/medium sand ($d_{50} = 0.25$ mm) and 15% mud/clay ($d_{50} = 0.035$ mm). A sediment source (500 g/m³) is introduced at the western boundary to prevent an over-erosion at the coastline close to the boundary. Compaction effects are not considered in the simulation. The real-time computation time step is 60 s for hydrodynamics and 180 s for suspended sediment transport. The time step for computation of bed-load transport is automatically determined within the model. Two experiments, named E01 and E02, are designed. Parameter settings are the same in these experiments except the setting of storms. E01 excludes storm effects and E02 includes a westerly storm with a return
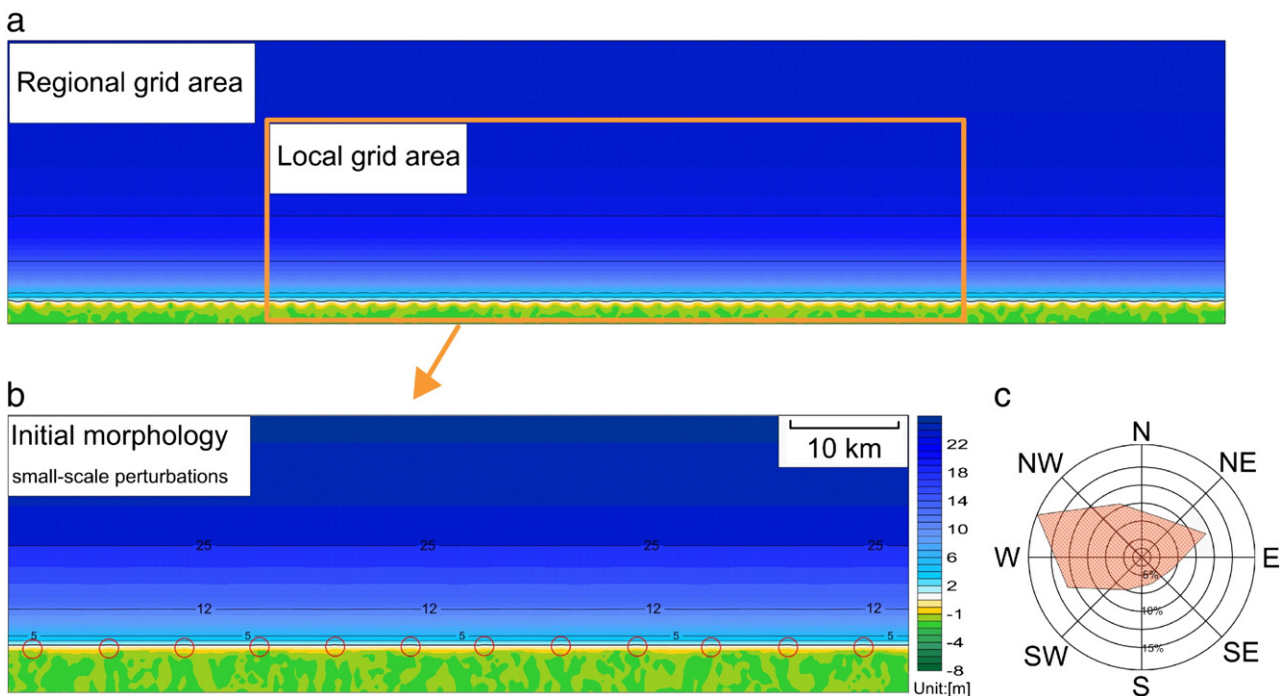

Fig. 4. (a): Coupled grids for the model. The regional grid is used to provide open boundary conditions (waves and currents) for the local grid; (b): Local grid area of interest. Red circles indicate small-scale perturbations at the coastline; and (c): Directional distribution of a synthetic wind spectrum for model input.

period of 1 year and an easterly storm with a return period of 5 years. Duration of the synthetic storms in E02 is 48 h. Wind speed starts from 14 m/s, increases linearly to 21 m/s and then decrease linearly to 14 m/s during the storm period. Two additional periods of 72 h of calm wind with a constant speed of 6 m/s are added, respectively, to both sides of the storm period in order to stabilize the computation. Direction of the wind is fixed at 292.5° (clockwise from the north) in the westerly storm and 67.5° in the easterly storm. No morphological update acceleration is used in storm simulation.

4.2. Model results and analysis

Simulation results of both experiments (E01 and E02) indicate that the formation of a spit is determined by the initial morphology of the coastline and the nearshore wave spectrum. Evolution of the spit system can be categorized into three periods according to the model results. The early period corresponds to a phase of fast development of the spit system from 0 to 500 years. The middle period corresponds to a phase of size competition between adjacent spits between 500 and 1500 years, and the late period corresponds to a phase of mergence of adjacent spits and development of large-scale spits after 1500 years.

4.2.1. Spit evolution in the early period

In the early period every initial perturbation of the coastline is amplified due to the effects of high-angle waves. On a sandy coast, the long-shore currents induced by wave-breaking are responsible for a major part of the nearshore sediment transport. Sediment transport flux is a non-linear function of radiation stress (which is explicitly determined by the wave strength and the incident wave angle relative to the contour line at the breaking point), bottom friction and sediment mobility. Instability in shoreline shape occurs when waves approach at a relative angle greater than that which maximizes sediment transport (Ashton et al., 2001). As the initial perturbation of the coastline causes varying incident wave angles along the surf zone, the long-shore sediment transport flux is variable and reaches a maximum at the place where the incident wave angle approaches 45°, and decreases if the wave directions deviate progressively farther from this angle. As the winds in the research area come mostly from W–NW, directions of incoming waves from offshore are dominated by a narrow spectrum. Maximum Sediment Transport Flux Sites, named MSTS hereafter, are formed under such condition in a particular area of each perturbation where the incident angle of dominant waves is close to 45° (as indicated by red ellipses in Fig. 5).

The spatially-variable long-shore residual sediment transport flux results in accretion at the down-drift side and erosion at the up-drift side of the MSTS. The incident wave angle at the down-drift side of the MSTS (which is greater than the maximum transport angle) gradually decreases due to the accretion; on the other hand, the erosion at the MSTS and its up-drift side also causes a decrease of the incident wave angle (which is smaller than the maximum transport angle). This makes the MSTS move down-drift toward the crest of the perturbation and causes an elongation of the crest. The perturbation therefore increases in size and gradually evolves into a spit. Fig. 6 shows the different phases through which a perturbation evolves into a spit. Results in Fig. 6 also indicate that the location of a perturbation/spit is not spatially fixed, but migrates along the residual sediment transport direction, which is eastward in our case. Such migration can also be explained by the shift of the MSTS.

The general behaviors of MSTS induce growth of the perturbations and small-scale spits are formed as a result. Fig. 7 shows the evolution of the research area during the early period in E01. The 12 m contour line serves as a closure depth on such a time-scale. Growth of the perturbations is almost homogeneous along the whole coastline. The small-scale spits develop a similar size until the end of this early period. Aeolian transport also plays an important role in the development of the spit system as it helps to stabilize the shape of the spit by building up sand dunes on the newly-formed land cells. On the other hand, aeolian landward transport induced by the dominant winds may also be a factor accelerating the erosion at some parts of the coastline. A major part of the terrestrial cells adjacent to the waterline becomes progressively 'thinner' due to the aeolian landward transport, which makes the coastline more vulnerable to strong wave attack.

Comparison of results between E01 and E02 indicates that storms play a positive role in the spit development in the early period. The spit system in E02 develops faster than that in E01 (Fig. 8). This is because storms erode more sediment from the coastline area than normal wind periods due to increased wave impacts combined with a high water stand. Most of such eroded sediment becomes deposited in the offshore area after a storm. Part of the deposited sediment is then transported alongshore during normal wind-climate periods to feed the growth of spits.
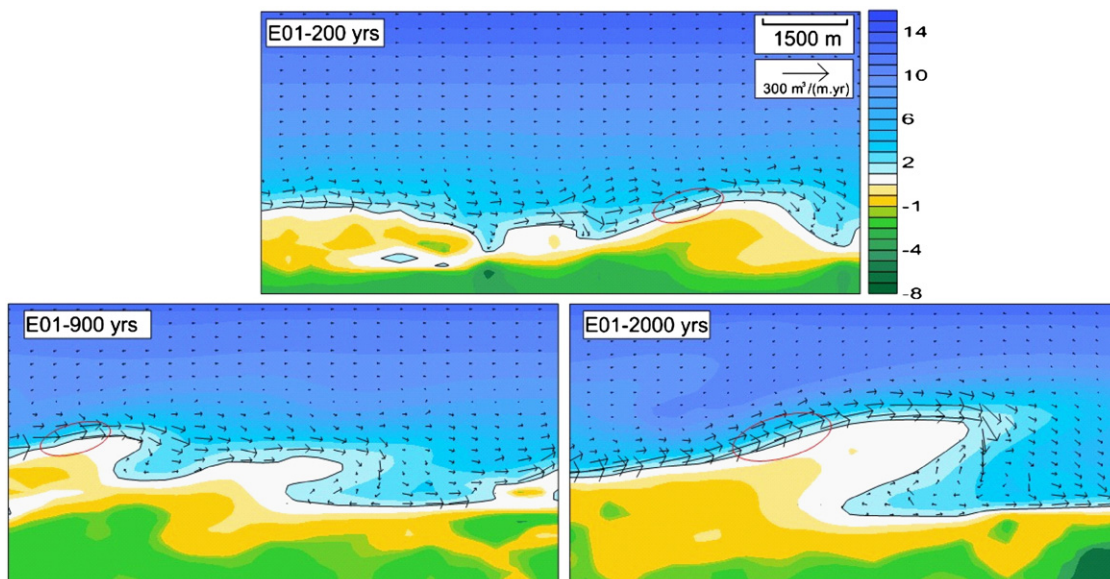

Fig. 5. Residual sediment transport flux at the perturbations/spits in different development ages. Vectors are plotted every four grid cells horizontally and every two cells vertically.
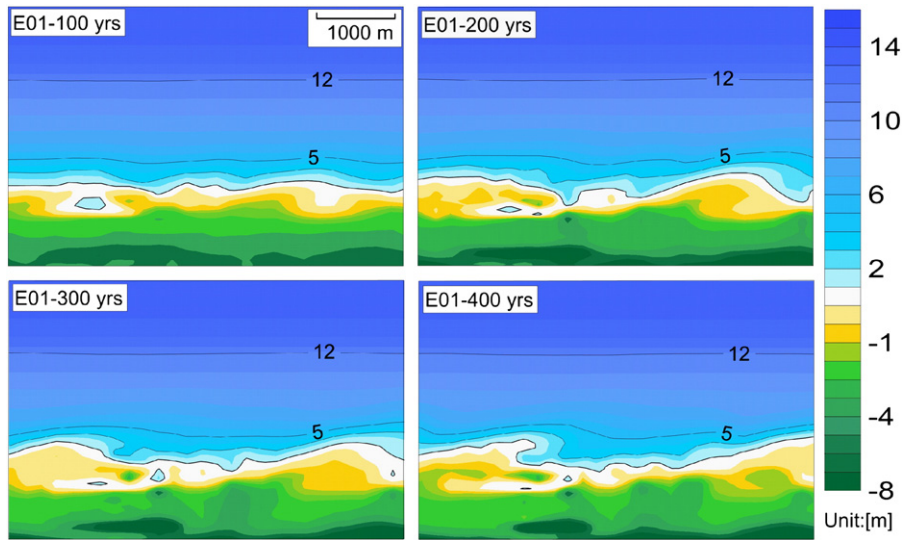
Fig. 6. Formation of a small-scale spit from a coastline perturbation.

4.2.2. Spit evolution in the middle period

When the small-scale spits grow to a certain size, their development is affected by their neighbors due to hydrodynamics and sediment transport. Interaction between adjacent spits starts and plays a progressively more important role in reshaping the spits. Size competition between adjacent spits dominates the middle period and development of the spits becomes progressively unbalanced. A larger-scale spit with abundant sediment supply from its up-drift area (determined by the residual effect, westward in our case) is able to migrate faster than its smaller down-drift neighbor. High-angle waves from the dominant direction spectrum are sheltered by the larger-scale spit when it migrates close enough to its neighbor (as shown in Fig. 5). Waves approaching the neighbor spit are transformed by this sheltering and cause two changes in characteristics: (1) high incident angle is no longer maintained, and (2) wave energy before breaking is reduced. The area of MSTS at the neighboring spit shrinks due to the sheltering effects and the residual long-shore sediment transport decreases. This results in a further reduction of the migration speed of the neighbor spit. In a latter phase of the middle period the larger-scale spit catches up with its smaller, slowly-moving neighbor and merge into one large-scale spit. Such evolution is shown in Fig. 9.
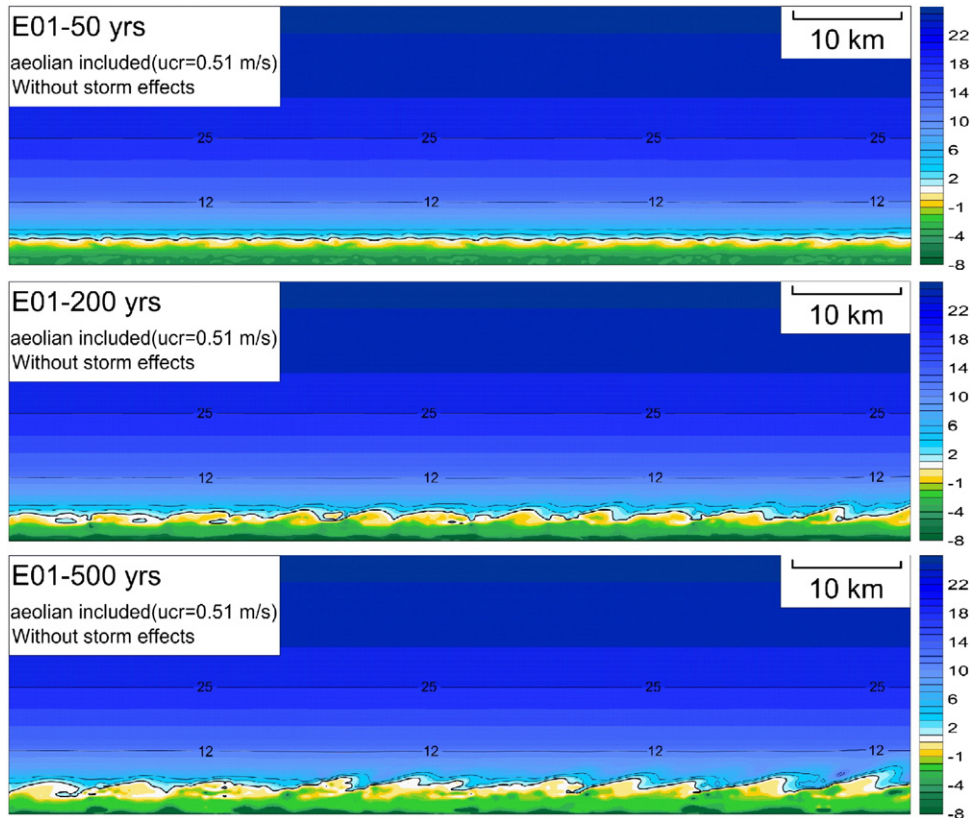

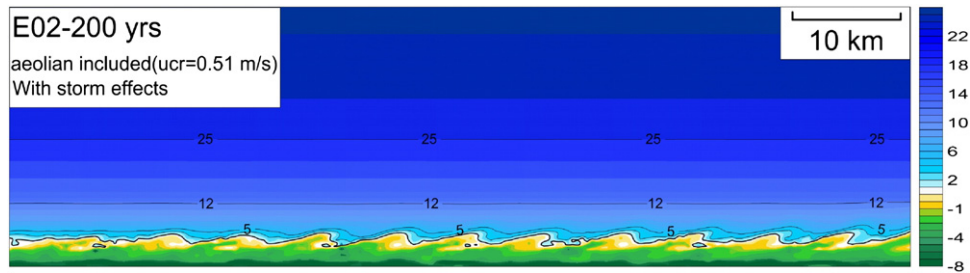**Fig. 7.** Evolution of the coastal morphology in the early age in Experiment 01.

Fig. 8. Evolution of the coastal morphology in the early age in Experiment 02.

Evolution of the whole research area shown in Fig. 10 indicates that development of the spit system in the middle period is no longer homogeneous. Seven relatively large-scale spits are formed by the end of the middle period from twelve original small-scale spits. Spits in the middle part of the system obtain a larger size than those close to the two ends. This is due to the effects of wind fetch. The research area is fetch-limited and, as long as the wind speed is larger than the wave phase speed, wave energy increases along its travel direction before the processes are finally dominated by bottom friction. As the research area is mostly driven by high-angle waves from W–NW, wave energy increases eastwards. The relatively low-energy waves in the western part of the system result in weaker radiation stresses at the surf zone than those in other parts, thus inducing less residual sediment transport flux along the coastline. With less residual sediment supply from the up-drift sides, spits in the western part evolve slower than those in other parts. On the other hand, although spits in the eastern part of the research area evolves faster than those in the middle and western part due to stronger wave effects, their sizes are limited by strong wave erosion. The spits in the middle part of the system, with an optimum wave environment for their growth, are able to develop largest in the system.

Simulation results from E02 (Fig. 11) indicate that storms play an opposite role in the middle period compared to the early stage. Spits develop more irregular shapes in E02 than those in E01 and the spit lengths are shorter. Such differences are caused by two factors: (1) aeolian transport continuously makes the terrestrial part of the coastline 'thinner' and vulnerable to strong wave erosion; and (2) storm erosion in the low-altitude part of the coastline causes irregular reshaping of the coastline and hinders the elongation of spits. Spits in E02 are thus shorter in length and broader in width than those in E01.

4.2.3. Spit evolution in the late period

After a relatively fast development in the early and middle period, the spit system evolves into a late period in which growth of the spits gradually slows down and more morphological features such as lagoons and barriers are developed (Fig. 12). Only four spits survive after 3000 years in E01. A large-scale spit is developed in the middle part of the system and remains stable on a millennial scale. Three smaller spits are developed in the eastern part, however, strong wave conditions in this area causes a continuous oscillation of the coastline and development of the spits are still far from equilibrium. Somewhat surprisingly, the western part of the coast has developed into a 'post-spit' phase in both simulations. Spits in the western part retrogress and are either smoothed or evolve into a barrier-lagoon environment. This is probably due to two facts: (1) the 'connectivity' of the coast increases when a barrier-lagoon forms, thus facilitating alongshore transport to the large eastern spit; and (2) the incoming sediment from the western open boundary is not sufficient to compensate the loss of sediment of the western coast, thus causing a retrogression of the coastline in this area. Comparing the results between the two experiments indicate that the barrier-lagoon (Fig. 12) has a shorter life period in E02 than in E01. This can be explained by the overwash effects during storms (E02), which transport large amounts of sediment from the outer coastline into the lagoon and gradually infill the space. The 12 m contour line also oscillates in this late period, indicating a larger closure depth on a millennial scale.

5. Discussion

Morphodynamic models which can be applied to long-term coastal evolution are still far from maturity (de Vriend, 2001; Fagherazzi
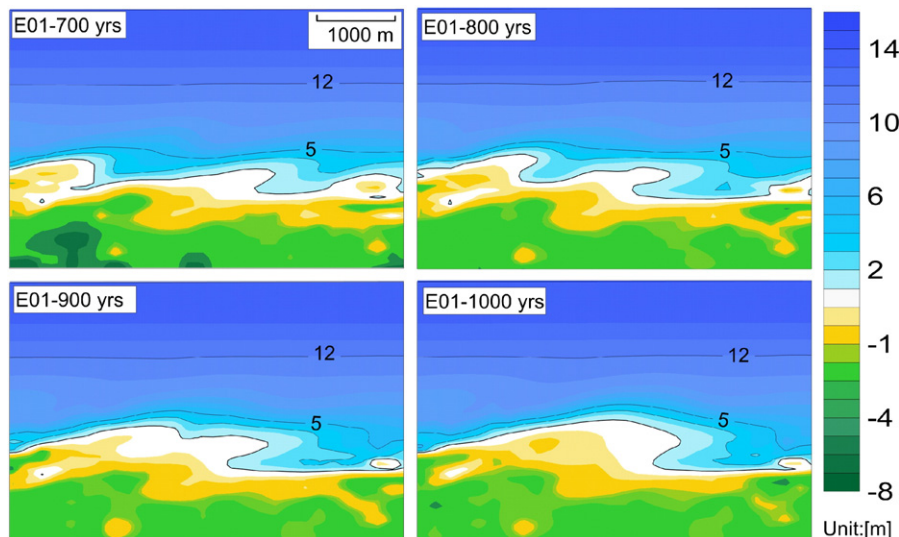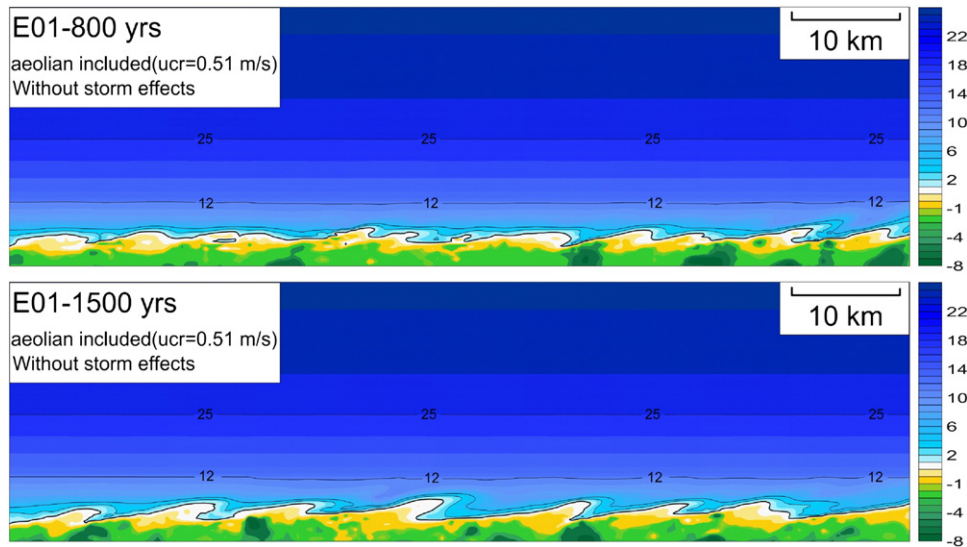

Fig. 9. Formation of a large-scale spit.

Fig. 10. Evolution of the coastal morphology in the middle period in Experiment 01.

and Overeem, 2007). There are two main obstacles: computational efficiency and model errors. Errors in a long-term simulation generally occur in two ways: numerical errors generated by the solver during a large number of iterations and systematic errors caused by biased inputs or due to limited knowledge of the system (Zhang et al., 2010). Considerable efforts have been made by the authors in the model construction to improve the computational efficiency and control the errors in a reasonable range. A parallel computation structure is applied to improve the computational efficiency. Representative climate driving conditions are introduced to simplify the model inputs. Different approaches, such as an additional diffusion, an Euler–WENO scheme, different evaluations of wave properties in the modules, a behavior-oriented evaluation of coastline change, a variable morphological update acceleration factor and long-term bathymetrical update strategies, are integrated in the code for a smooth evolution of the coastal morphology. Hybrid coupling of process-based modules and behavior-oriented formulations is used to solve multi-scale processes in a pre-designed grid system. A large number of experimental runs were carried out to test the sensitivity of simulation results to different parameter settings. This helps to obtain the best sets of parameters that produce a coastline change close to observations. Sensitivity studies also help to quantify the effects of different driving mechanisms on the long-term coastal evolution. Therefore, they enable us to evaluate the model performance and capture the main driving processes that dominate the morphological evolution at the scales of interest. A modeling methodology integrated by the above measures, which has been applied to a real case — the Darss–Zingst peninsula in the southern Baltic Sea, seems to provide a feasible way for numerical simulation of general long-term morphological evolution of wave-dominated coasts.

Although the simulations in Section 4 are based on an ideal setting of the initial parameters and constant periodic climate driving conditions, similar morphological features like those obtained in the simulation can be found in nature. An example for spit development in fetch-limited environment is described by Ashton et al. (2001) in the Sea of Azov, Ukraine. Spits in the eastern part of the coast are smaller in size than those in the middle and western part due to weaker wave forcing. Although the spit in the western part develops a longest length in the system, it is fragile without anthropogenic protection due to insufficient sediment supply from its shoreface and could be easily breached by storm erosion. The spits in the middle part, similar to our case, develop a shoreface with the largest size in the system, which ensures a stable further development.

Simulation results indicate that the model is able to produce reasonable long-term morphodynamics of wave-dominated sandy coasts that are consistent with general coastal behaviors in nature. We present only simulation results from two ideal settings, i.e. with and without storm effects, in the text for a comparative study, though there are other factors which have significant influences on long-term coastal evolution, for instance, sea-level change and isostatic crustal movements. The impacts of relative sea-level change are included in the application to the real coast and they are revealed as important factors for the barrier development (Harff et al., 2011; Zhang et al., submitted for publication). Sensitivity studies of impacts of the sea-level change on long-term evolution of the ideal coast are illustrated in the supplementary online material. Results indicate that only moderate sea-level change rates, with either positive or negative values, allow further development of the spit system in which large scale spits are formed. A high rate of sea-level change (e.g. ±3 mm/a) acts as a hindering factor for spit development over the long term.
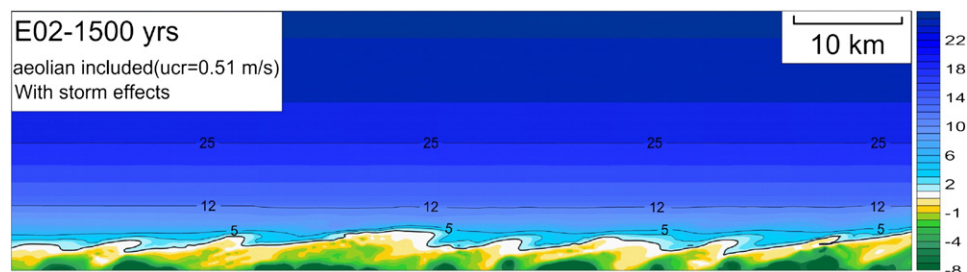

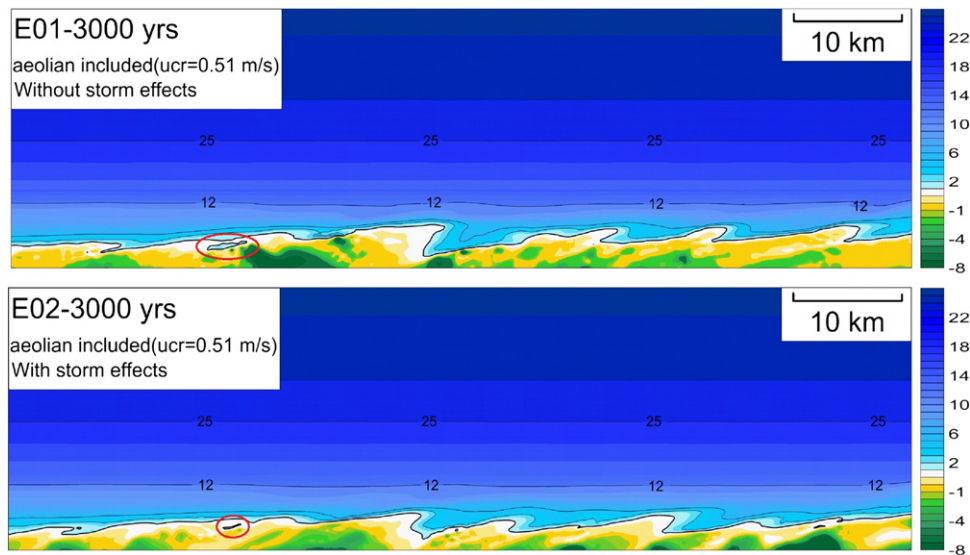**Fig. 11.** Evolution of the coastal morphology in the middle period in Experiment 02.

Fig. 12. Evolution of the coastal morphology in the late period in Experiment 01 and Experiment 02. Red ellipses indicate the barrier-lagoon.

Despite its robustness, there are still some shortcomings that need to be addressed. The first is related to the scales that the model is applicable to. The model produces satisfactory results on decadal-to-millennial timescales by the use of representative time series, rather than real time series from measurements, as driving conditions. The representative time series are extracted from measurements that cover a relatively long time span (such as decades) and are fine-tuned by sensitivity studies (one example is given in Zhang et al., 2010a) to approximate the long-term morphological change. Oscillations of driving mechanisms may occur on a short-term scale such as seasonal and annual scale, and this can induce non-linear effects on the morphological change which cannot be reflected by representative time series. The spatial scale that the model is applicable to is also restricted to medium to large by the physical processes resolved in the model. Three-dimensional or small spatial scale (several to tens of meters) processes, such as coastal upwelling and downwelling, density currents and undertow, are not resolved in the vertically-averaged model. This causes invalidity of the model when it is applied to an area dominated by processes acting on three-dimensional or small spatial scales.

The second shortcoming of the model is an underestimation of the coastline erosion between two adjacent spits. The coastline between two growing spits usually presents a concave shape in nature due to wave erosion and insufficient sediment supply (as most sediment is trapped in the spit crest area), however, this feature is not well reflected in our simulation. This is due to an underestimation of wave energy when waves enter the sheltering area from the crest of the spit. The underestimated wave energy results in a relatively weak residual sediment transport (as shown in Fig. 5), thus is not able to cause significant erosion of the coastline. More accurate wave transport formulation is therefore needed to be integrated in the model to approximate the wave transformation in sheltered shallow water areas. Another shortcoming of the model is related to the coastal dune dynamics. The model seems not being able to produce long and thin spits. Although these kinds of spit are fragile and can be easily destroyed by storm breaching, they exist in nature and their presence may be due to the following preconditions: 1. a sufficient sediment supply from the shoreface and the up-drift side of the spit; 2. a mild nearshore wave climate that dominated by high-angle incident waves; 3. low-frequency or no storms; 4. a long-term stable sea level; and 5. protection by sand dunes at the front of the coast (so-called frontal dunes). Our model is able to satisfy most of

the preconditions, except the last one. Formation of frontal sand dunes is not well reflected in the model results due to two factors: (1) the frontal dunes in nature usually present a long length along-shore but short width in the cross-shore direction, which is not spatially resolved by the resolution of our model; and (2) mechanisms for formation of frontal sand dunes are not well formulated in the model, especially the vegetation effects and the air-flow circulation at the back of a frontal dune which helps to build up the dune. Without protection of frontal sand dunes at the coastline, a further elongation of the spits is hindered by wave erosion. More studies will be necessary to improve the description of coastal dune dynamics in our future work.

6. Conclusions

A hybrid morphodynamic model, which combines process-based modules based on conservative equations to solve the transport of waves, currents, sub-aqueous sediment and behavior-oriented modules based on empirical descriptions of cliff erosion, bed-load and terrestrial aeolian sand transport, is constructed in a parallel code to simulate decadal- to millennial-scale morphological evolution of wave-dominated coasts. Several approaches are implemented in the model to ensure a smooth evolution of the morphology during a large number of iterations for long-term computations. An application of the model to a real coast, the Darss–Zingst peninsula at the southern Baltic Sea, indicates that the model is able to reproduce the main morphological features of the barrier system on a millennial temporal scale. An idealized fetch-limited sandy coast and a synthetic wind series which induces a predominant high-angle nearshore wave spectrum are then designed for a model study to investigate the morphogenesis and evolution of a general wave-dominated coastal system. Simulation results indicate that the model is able to produce reasonable long-term morphodynamics of wave-dominated sandy coasts that are consistent with general coastal behaviors in nature. Analysis of results indicates that evolution of a sandy spit system in a fetch-limited environment can be classified into three different periods. Comparative studies of the long-term significance of storms indicate that storms affect the spit development differently in different periods. They facilitate the formation of spits in the early stage and tend to hinder their further growth later. Simulation results also indicate that the terrestrial aeolian transport not only plays a key role in stabilizing the spits by building-up sand dunes but are also

responsible for long-term erosion of the coastline. The model can also be applied to more complex wave-dominated coastal types, such as cliff coasts, with careful consideration of sediment components and resistant strength of the coastline boundary.

Acknowledgments

Appendix A. Supplementary data

Supplementary data to this article can be found online at doi:10.1016/j.geomorph.2012.01.019.

References

Antunes do Carmo, J.S., Seabra-Santos, F.J., 2002. Nearshore sediment dynamics computation under the combined effects of waves and currents. Advances in Engineering Software 33, 37–48.
Ashton, A., Murray, A.B., Arnault, O., 2001. Formation of coastline features by large-scale instabilities induced by high-angle waves. Nature 414, 296–300.
Cayocca, F., 2001. Long-term morphological modeling of a tidal inlet: the Arcachon Basin, France. Coastal Engineering 42, 115–142.
Chiang, Y.C., Hsiao, S.S., Lin, M.C., 2010. Numerical solutions of coastal morphodynamic evolution for complex topography. Journal of Marine Science and Technology 18, 333–344.
Dastgheib, A., Roelvink, J.A., Wang, Z.B., 2008. Long term process-based morphological modelling of the Marsdiep tidal basin. Marine Geology 256, 90–100.
de Vriend, H.J., 2001. Long-term morphological prediction. In: Seminara, G., Blondeaux, P. (Eds.), River, Coastal and Estuarine Morpho-dynamics. Springer, Berlin, pp. 163–190.
de Vriend, H.J., Copabianco, M., Chesher, T., De Swart, H.E., Latteux, B., Stive, M.J.F., 1993a. Long term modelling of coastal morphology. Coastal Engineering 21, 225–269.
de Vriend, H.J., Zyserman, J., Nicholson, J., Roelvink, J.A., Pechon, P., Southgate, H.N., 1993b. Medium term 2DH coastal area modelling. Coastal Engineering 21, 193–224.
Dissanayake, D.M.P.K., Roelvink, J.A., 2007. Process-based approach on tidal inlet evolution—part 1. Proceedings RCEM conference, Vol.1. Enschede, The Netherlands, pp. 3–9.
Dong, Z.B., Liu, X.P., Wang, H.T., Wang, X.M., 2003. Aeolian sand transport: a wind tunnel model. Sedimentary Geology 161, 71–83.
Fagherazzi, S., Overeem, I., 2007. Models of deltaic and inner continental shelf landform evolution. Annual Review of Earth and Planetary Science 35, 685–715.
Fortunato, A.B., Oliveira, A., 2007. Improving the stability of a morphodynamic modeling system. Journal of Coastal Research SI50, 486–490.
Grant, W.D., Madsen, O.S., 1979. Combined wave and current interaction with a rough bottom. Journal of Geophysical Research 84, 1797–1808.
Hanson, H., Aarninkhof, S., Capobianco, M., Jiménez, J.A., Larson, M., Nicholls, R.J., Plant, N.G., Southgate, H.N., Steetzel, H.J., Stive, M.J.F., de Vriend, H.J., 2003. Modelling of

coastal evolution on yearly to decadal time scales. Journal of Coastal Research 19, 790–811.
Harff, J., Zhang, W.Y., Meyer, M., Schneider, R., 2011. Coastline change—from paleoenvironmental reconstruction to future scenarios: a case study from the Baltic. ASCE conference proceedings, Anchorage, Alaska, pp. 164–175.
Harten, A., Engquist, B., Osher, S., Chakravarthy, S., 1987. Uniformly high-order accurate essentially non-oscillatory schemes, III. Journal of Computational Physics 71, 231–303.
Hünicke, B., Zorita, E., Haeseler, S., 2010. Baltic Holocene climate and regional sea-level change: a statistical analysis of observations, reconstructions and simulations within present and past as analogues for future changes. GKSS Report 2010/2. 70 pp.
Jiménez, J.A., Arcilla, A.S., 2004. A long-term (decadal scale) evolution model for micro-tidal barrier systems. Coastal Engineering 51, 749–764.
Johnson, H.K., Zyserman, J.A., 2002. Controlling spatial oscillations in bed level update schemes. Coastal Engineering 46, 109–126.
Karunarathna, H., Reeve, D., Spivack, M., 2008. Long-term morphodynamic evolution of estuaries: an inverse problem. Estuarine, Coastal and Shelf Science 77, 385–395.
Lampe, R., 2002. Holocene evolution and coastal dynamics of the Fischland–Darss–Zingst peninsula. Greifswald Geographische Arbeiten 27, 155–163.
Latteux, B., 1995. Techniques for long-term morphological simulation under tidal action. Marine Geology 126, 129–141.
Lettau, K., Lettau, H.H., 1978. Experimental and micro-meteorological field studies of dune migration. In: Leattau, H.H., Lettau, K. (Eds.), Exploring the World's Driest Climate. IES Report, vol. 101. University of Wisconsin, Madison, pp. 110–147.
Liu, X.D., Osher, S., Chan, T., 1994. Weighted essentially non-oscillatory schemes. Journal of Computational Physics 115, 200.
Long, W., Kirby, J.T., Shao, Z., 2008. A numerical scheme for morphological bed level calculations. Coastal Engineering 55, 167–180.
Masetti, R., Fagherazzi, S., Montanari, A., 2008. Application of a barrier island translation model to the millennial-scale evolution of Sand Key, Florida. Continental Shelf Research 28, 1116–1126.
Roelvink, J.A., 2006. Coastal morphodynamic evolution techniques. Coastal Engineering 53, 277–287.
Roelvink, J.A., Reniers, A.D., van Dongeren, A.P., van Thiel de, V.J., McCall, R., Lescinski, J., 2009. Modelling storm impacts on beaches, dunes and barrier islands. Coast Engineering 56, 1133–1152.
Schumacher, W., 2002. Coastal evolution of the Darss Peninsula. Greifswalder Geographische Arbeiten 27, 165–168.
Watanabe, A., Maruyuma, K., Shimizu, T., Sakakiyama, T., 1986. Numerical prediction model of three-dimensional beach deformation around a structure. Coastal Engineering in Japan 29, 179–194.
Wu, C.Y., Ren, J., Bao, Y., Lei, Y.P., Shi, H.Y., He, Z.G., 2007. A long-term hybrid morphological modeling study on the evolution of the Pearl River delta, network system and estuarine bays since 6000 aBP. In: Harff, J., Hay, W.W., Tetzlaff, D.F. (Eds.), Coastline Changes: Interrelation of Climate and Geological Processes: Geological Society of America, Special Paper, 46, pp. 199–214.
Zhang, W.Y., Harff, J., Schneider, R., Wu, C.Y., 2010. Development of a modeling methodology for simulation of long-term morphological evolution of the southern Baltic coast. Ocean Dynamics 60, 1085–1114.
Zhang, W.Y., Harff, J., Schneider, R., 2011a. Analysis of 50-year wind data of the southern Baltic Sea for modelling coastal morphological evolution — a case study from the Darss–Zingst Peninsula. Oceanologia 53 (1-TI), 489–518.
Zhang, W.Y., Harff, J., Schneider, R., Wu, C.Y., 2011b. A multi-scale centennial morphodynamic model for the southern Baltic coast. Journal of Coastal Research 27, 890–917.
Zhang, W.Y., Harff, J., Schneider, R., Meyer, M., Zorita, E., Hünicke, B., submitted for publication. Holocene morphogenesis at the southern Baltic Sea: simulation of multi-scale processes and their interactions for the Darss–Zingst peninsula. Journal of Marine Systems.